ELSEVIER

Contents lists available at ScienceDirect

Materials Science & Engineering C

journal homepage: www.elsevier.com/locate/msec



A facile method to synthesize mussel-inspired polydopamine nanospheres as an active template for in situ formation of biomimetic hydroxyapatite



Farnaz Ghorbani^a, Ali Zamanian^{b,c,d,*}, Aliasghar Behnamghader^b, Morteza Daliri Joupari^e

- ^a Department of Biomedical Engineering, Science and Research Branch, Islamic Azad University, Tehran, Iran
- ^b Department of Nanotechnology and Advanced Materials, Materials and Energy Research Center, Karaj, Iran
- ^c Stem cell Research Center, Tehran University of Medical Sciences, Tehran, Iran
- ^d Department of Biomaterials, Aprin Advanced Technologies Development Company, Tehran, Iran
- e Department of Animal, Avian and Marine Biotechnology, National Institute of Genetic Engineering and Biotechnology, Tehran, Iran

ARTICLE INFO

Keywords: Polydopamine Nanosphere Mussel-inspired Bioactivity Hydroxyapatite Biomimetic

ABSTRACT

In this study, Mussel-inspired polydopamine (PDA) nanospheres were synthesized via spontaneous oxidative polymerization of dopamine hydrochloride (dopa-HCl) in a deionized water-alcohol mixed solvent at room temperature and atmospheric air, under alkaline condition. Field-emission scanning electron microscopy (FE-SEM) demonstrated production of sphere-like shape with a smooth surface and tunable size, while monodispersity increased by utilizing isopropanol instead of ethanol owing to lower R_a values based on Hansen solubility parameter (HSP) theory. Dropwise addition of monomer played an undeniable role in the fabrication of uniform and smaller spheres. The difference of the charge repulsion of constructs in the range of pH led to different dispersive behavior in a variety of solvents, exhibiting versatile applications. The presence of active functional groups on the surface of PDA spheres made them an appropriate option for PDA-assisted biomimetic mineralization of hydroxyapatite (HA), which is the result of the interaction between abundant catecholamine moieties in PDA and Ca^{+2} ions in simulated body fluid. Bio-adhesive nature of PDA in water and the presence of amino and hydroxyl functional groups support desirable L929 mouse fibroblast cell spreading. The viability of > 90% fibroblast cells proved the biocompatibility of polymerized structure. All the achievements indicated that PDA nanospheres provide a biocompatible and bioactive template for green synthesizing hydroxyapatite and the innovative basis for further tissue engineering applications.

1. Introduction

The materials used in replacement of the functions in injured tissues should be biocompatible and categorized into four major sections of polymers, ceramics, metals, and composites [1]. Among the broad range of materials, nanoscale structures such as carbon nanotube [2], nano silica [3], graphene-based structures [4], silver nanoparticles [5], nanogold [6], magnetic nanoparticles [7], etc., with the capability to control size, shape, morphology [8], and chemical composition are attractive to many scientists. Ameliorated mechanical, electrical, and optical properties of these ultra-fine materials compared to other constructs have led to defining the diversity of applications [9]. However, great biocompatibility and generating a minimal inflammatory response, flexibility, controllable biodegradability, etc., of nanoscale polymers have made them applicable for several performances [10–12]. Nonetheless, the restricted mechanical stability of polymeric structures has made scientists turn to organic-inorganic hybrid constructs. In

recent years, dopamine which is a hormone and neurotransmitter [13] in the human body has been developed for biological usage. It is an inspired material based on adhesive proteins in mussels [14] containing catecholamine groups [15]. This melanin-like material has expanded in typical applications such as surface coating [16], drug delivery [17], tissue engineering [18], etc. Besides, polydopamine (PDA) micro/nanospheres that can be obtained via spontaneous oxidative polymerization have received lots of attention in biomedical areas due to its unique properties [19,20]. Environmentally friendly, bioactivity and capability to functionalize with other materials [21], hydrophilicity, bio-adhesion [22,23], lack of restriction on size, uniform spherical shape [23], thermal stability, facile and cost-effective synthesizing [24], non-toxicity [13], etc., are fantastic features of this material which induces a widespread influence on its usage. The solvent used in polymerization has effects on the chemical synthesizing of PDA spheres. Therefore, Jiang et al. [25] investigated the effect of different water-based media in order to choose an optimal reaction media. Their investigation

^{*} Corresponding author at: Department of Nanotechnology and Advanced Materials, Materials and Energy Research Center, Karaj, Iran. E-mail address: a-zamanian@merc.ac.ir (A. Zamanian).

indicated that mixed solvents promise more uniformity in structure of spheres because of the similarity of the media with naturally occurring reactions.

Biomineralization refers to the ability of constructs to attract simulated body fluid (SBF) ions for nucleation of hydroxyapatite (HA)like layers at physiological temperature and pH as a function of time [2,9,26], while the concentration of SBF ions can affect the amount of constructed crystalline layers and Ca/P ratio [27,28]. Scientists reported that crystallinity of these layers could be controlled by pH and ionic strength of SBF [29-31]. PDA sphere is one of the bioactive nanoparticles so that the enhanced mineralization capability exhibited in SBF is due to the inherent chemical activation that provides a situation for catecholamine functional groups to interact with metal ions in SBF and formation of biomimetic mineralized layers [32]. Cui et al. [33] functionalized polystyrene (PS) nanoparticle via PDA. They fabricated hybrid construct via soaking the coated nanoparticles in SBF to synthesize biomimetic HA. In fact, modification of PS changes its inert behavior to bioactive and enables best possible template for biomineralization. Zhe et al. [34] induced HA mineralization on the surface of anodized titanium via PDA modification after soaking the constructs in $1.5 \times$ SBF solution. Their results indicated that biomimetic formation of HA enhances corrosion resistance and wettability of samples. Stimulating the cellular attachment and alkaline phosphatase expression is another achievement of their study. Cheng et al. [35] precipitated HA on polycaprolactone scaffolds after modification via PDA. Their results demonstrated that adsorption of extracellular matrix increased considerably on PDA coated samples. Moreover, focal adhesion kinase levels and secretion of human mesenchymal stem cells increased as a function of PDA concentration.

Herein, mussel-inspired PDA nanospheres were fabricated via spontaneous oxidation of dopamine hydrochloride (dopa-HCl) under alkaline condition, in atmospheric air and ambient temperature. The synthesizing procedure was performed in mixed water-alcohol solution, and the effect of different alcohols (ethanol and isopropanol) in the production of uniform and monodisperse spheres were characterized. Moreover, the influence of direct and dropwise addition of monomer to mixed solvent was investigated in this study. Then, the mechanism of polymerization and biodegradation procedure were determined through further analysis. The capability of PDA for the biomimetic formation of HA in SBF solution was proved in the present study. Finally, biological evaluation of the nanospheres was examined via cell adhesion and MTT assays.

2. Experimental

2.1. Materials

Dopamine hydrochloride (dopa-HCl, $M_w = 189.64 \text{ g/mol}$, Glutaraldehyde (25%, d = 1.058 g/cm³), Hydrochloric acid (HCl, 37%, $M_{\rm w} = 36.46 \, \text{g/mol}$), and Potassium Hydrogen Phosphate Trihydrate (KHPO $_4$:3H $_2$ O, M $_w$ = 228.22 g/mol) were purchased from Merck Co. Ltd. (Germany). Thiazolyl Blue Tetrazolium Bromide (MTT, M_w = 414.32 g/ mol), Dimethyl Sulfoxide (DMSO, $1\times$), and L-Glutamine ($M_w = 146.14 \, g/$ mol) were purchased from Sigma Co. Ltd. (USA). Isopropanol (99.99%, $M_w = 60.10 \text{ g/mol}$), ethanol (99.8%, $M_w = 46.07 \text{ g/mol}$), Tris(hydro $xymethyl)aminomethane (M_w = 121.14 g/mol), Sodium hydroxide$ (NaOH, $M_w = 40.00 \text{ g/mol}$), Sodium chloride (NaCl, $M_w = 58.44 \text{ g/mol}$), Potassium chloride (KCl, M_w = 74.55 g/mol), Sodium bicarbonate (NaHCO₃, $M_w = 84.01$ g/mol), Calcium chloride (CaCl₂, $M_w = 110.98$ g/ mol), Magnesium chloride hexahydrate (MgCl₂·6H₂O, M_w = 203.30 g/ mol), and Sodium sulfate anhydrous (Na₂SO₄, M_w = 142.04 g/mol) were purchased from Samchun Pure Chemicals CO. Ltd. (Korea). Phosphate buffer saline (PBS, dry powder) was purchased from Aprin Advanced Technologies Development Co. Ltd. (Iran). Dulbecco's Modified Eagle's Medium (DMEM), Fetal bovine serum (FBS), penicillin-streptomycin were purchased from Gibco-BRL, Life Technologies Co. Ltd. (NY). Osmium

 Table 1

 Composition and characterization of PDA nanospheres.

Code	Water:alcohol ratio	dopa-HCl concentration (mg/mL)	Monomer addition	Average diameter (nm)
PDAEP	5:1	1.5	Directly	673.62 ± 168.75
PDAED	5:1	1.5	Dropwisly	660.36 ± 128.57
PDAIP	5:2	1.5	Directly	490.66 ± 25.48
PDAID	5:2	1.5	Dropwisly	441.80 ± 24.04

tetroxide was purchased from Polyscience, Warmington Co. Ltd. (USA). All chemicals were utilized directly without further purification. Aqueous solutions were prepared with deionized (DI) water.

2.2. Synthesis of PDA nanospheres

PDA nanospheres were synthesized by the oxidative polymerization of dopa-HCl in alkaline solution. Briefly, alcohol (ethanol, isopropanol) mixed with DI-water. Tris-buffer solution ($10\,\mathrm{mM\cdot L^{-1}}$) was added to the mixture of alcohol/water under gentle stirring (250 rpm). pH was adjusted on 8.5 by adhesion of HCl (1 M). Finally, dopa-HCl was added to the prepared solution with the concentration of 1.5 mg/mL (based on DI-water) directly and dropwise. Dropwise addition of dopa-HCl was followed by the rate of 30 drops/min. The solution turned to pale brown and gradually dark brown. The final blend was stirred for 72 h at room temperature in dark room. The products were centrifuged (NF1200R, NÜVE Co. Turkey) with DI-water at 9000 rpm for three times and were lyophilized in a freeze dryer (FD-10, Pishtaz Engineering Co. Iran) for 48 h at a temperature of $-58\,^{\circ}\mathrm{C}$ and pressure of 0.5 Torr. Finally, dry black powder was prepared. Table 1 represents all the details of nanosphere preparation.

2.3. Methods

2.3.1. Morphology observation

The morphological evaluation of the PDA nanospheres was determined using field-emission scanning electron microscopy (FE-SEM, MIRA3, TESCAN Co., Czech Republic) at an accelerating voltage of 15 kV. So, polymeric samples were sputter-coated with a thin layer of gold by sputtering (Emitech K450X, Ashford, UK) in 120 s continuous cycle at 45 mA to reduce charge density and create a conductive surface.

2.3.2. Size distribution

The average size of nanospheres was characterized by Image measurement software (KLONK Image Measurement Light, Edition 11.2.0.0), and measuring the diameter of 25 spheres in five FE-SEM micrographs with a magnification of 20 KX.

The hydrodynamic diameter of PDAID nanospheres was determined by dynamic light scattering (DLS, MAL1001767, Malvern Instruments, UK) at the temperature of 25 $^{\circ}\text{C}$ in ethanol.

2.3.3. Polymerization

Variation of pH during synthesis process was followed by pH meter (P25, Istek Co., Korea) at 1, 2, 3, 4, 5, 6, 24, 48, and 72 h after addition of dopa-HCl to pH-adjusted water/alcohol solution.

Fourier transforms infrared spectrophotometer (FTIR, Nicolet Is10, Thermo Fisher Scientific, USA) was used to determine the chemical characterization of the raw materials and nanospheres. So, 2 mg of the samples was carefully mixed with 100 mg of KBr (infrared grade) and pelletized under vacuum. Then, pellets were characterized by the wavenumber of 400 to $4000\,\mathrm{cm}^{-1}$ with a resolution of $4.0\,\mathrm{cm}^{-1}$ and 8 scans.

The proton nuclear magnetic resonance (H-NMR) spectra were obtained to ensure about polymerization of dopa-HCl. Therefore, samples

were dissolved in deuterium oxide (D_2O):DMSO- d_6 (1:1) and introduced into NMR tube. A 4 mm MAS probe was utilized in spectroscopy at an applied frequency of 5000 Hz. The measurements were conducted on NMR spectrometer (ECX 400, JEOL Co., USA) at a temperature of 303 K.

2.3.4. Zeta potential

The effect of pH on charge density of the PDA nanospheres was performed by determining zeta potential at a variety of pH and using a zeta sizer (Nano ZS, Malvern Co., UK) at a humidity of 20% and pressure of 1 atm at room temperature. Therefore, 1 mg of nanospheres was dispersed in 50 mL DI-water (pH 7) under ultrasonication (WUC-D10H, WISD Co., South Korea). The pH of the solution was adjusted in the range of 3–10 by the addition of HCl (1 M) and NaOH (1 M) dropwise.

2.3.5. In-vitro biodegradation

In-vitro biodegradation behavior of the samples was examined according to the results of FE-SEM, FTIR spectrum, ultraviolet-visible absorption (UV-vis, Lambd25, Perkin-Elmer Co., USA) spectroscopy, and thermal gravimetry (TGA, TGA 209 F1, Netzsch Co., Germany) analysis. Hence, 20 mg of the polymeric nanospheres was immersed in 50 mL PBS solution (pH 7.4), and the samples were placed in a thermoshaker (LS-100, Thermo Scientific, USA) with the rotational speed of 30 rpm and constant temperature at 37 \pm 0.5 °C for 4 weeks. PBS solution was refreshed every week. At the end of the experiment, nanospheres were washed with DI-water and lyophilized in a freeze dryer (temperature about $-58\,^{\circ}\text{C}$ and pressure 0.5 Torr for 24 h). Morphological evaluation and chemical characterization were followed as described above. UV-vis spectrum of the samples before and after biodegradation was monitored at the range of 150-650 nm. TGA was performed under an air atmosphere at a pressure of 1 atm and a heating rate of 10 °C/min.

2.3.6. Bioactivity

The ability of the nanospheres to support mineralization of hydroxyapatite was carried out by immersion of 20 mg PDA samples in 50 mL SBF (pH7.3) for 14 and 28 days as described by Kokubo et al. [36] (Table 2). The SBF-immersed spheres were placed in a thermoshaker under shaking at 37 \pm 0.5 °C and the rotational speed of 30 rpm. The SBF solution was refreshed every 2 days until the end of the experiment. Finally, PDA spheres were washed by DI-water and lyophilized in a freeze dryer (temperature about -58 °C and pressure 0.5 Torr for 24 h). The surface morphology and elemental analysis of the samples were evaluated using FESEM-EDX. The absorbance peaks were detected by UV-vis spectrum in the range of 200-600. Phase analysis of the polymeric constructs was conducted using an X-ray diffraction (XRD, PW3710, Philips Co., Netherlands). Results were obtained in the range of 2θ (5-65°) using Cu-Kα radiation under the operating conditions of 40 kV and 30 mA. XRD patterns compared with JCPDS standards to identify the crystalline phases. FTIR spectrum was used to show the chemical peaks related to the formation of hydroxyapatite. Monitoring pH during hydroxyapatite formation was followed by pH meter every other day without refreshing SBF solution. The variation of surface

Table 2Ion concentration of SBF compared with human blood plasma.

Ion	Blood plasma concentration (mM)	SBF concentration (mM)
Na ⁺	142.0	142.0
K ⁺	5.0	5.0
Mg ²⁺ Ca ²⁺	1.5	1.5
Ca ²⁺	2.5	2.5
Cl ⁻	103.0	147.8
HCO ₃	27.0	4.2
HPO_4^{2-}	1.0	1.0
SO ₄ ²⁻	0.5	0.5

roughness after mineralization was evaluated by atomic force microscopy (AFM, Rasterscope C26, DME Co., Denmark) technique. 1 mg of nanospheres was dispersed in 5 mL of ethanol under ultrasonication. A droplet of the solution was deposited onto cleaved mica and then measured by STM mode t Resonance frequency of 50–105 kHz and force constant 0.15–1.5 N/m.

2.4. Cells-spheres interactions

The biological behavior of PDA nanospheres was evaluated using L929 mouse fibroblast cells supplied by Materials and Energy Research Center (MERC) cell bank (Alborz, Iran). Nanospheres were sterilized by washing with sterile PBS 0.1 M (3 times), soaking in PBS-diluted penicillin-streptomycin 4h at room temperature, again washing and soaking in sterile PBS 0.1 M for 3 times and 24 h at 4 °C, respectively. Then, 5×10^4 cells/mL third passage of cells were combined with 5 mg aseptic samples. Cell loaded samples were covered by DMEM supplemented with 15% FBS, 100 g/mL penicillin-streptomycin, and 1.2% glutamine and incubated (Incubator, MCO-19ALC, SANYO Co., Japan) at 37 °C, 5% CO2, and 95% humidity for 3 h. Every 30 min the suspension was stirred at 30 rpm for 2 min. After removal of the culture medium, the cell-loaded spheres were rinsed in PBS three-time and were centrifuged at 300g for 5 min. The cells were fixed in 3% glutaraldehyde solution. After 30 min, the samples were rinsed again in PBS at 40 °C. Nanospheres were then fixed with 1% osmium tetroxide followed by dehydration with ethanol solutions of ascending concentrations (i.e., 30, 50, 70, 90, and 100%) for about 20 min at each one. The samples were then let dry in air, coated with gold, and observed by FE-SEM to evaluate cellular adhesion.

The proliferation of L929 cells on PDA nanospheres was investigated by MTT (3-{4,5-dimethylthiazol-2yl}-2,5-diphenyl-2H-tetrazolium bromide) assay as described in published work [37]. Briefly, the medium was removed, 2 mL MTT/cell culture medium (1:5) solution was added to each well, and was incubated at 37 °C for 2 h in a fully humidified atmosphere at 5% CO₂. The medium was discarded and precipitated formazan was dissolved in DMSO. The optical density (OD) of the samples, as a cell viability indicator, was measured by ELISA (enzyme-linked immunosorbent assay) reader at a wavelength of 570 nm with a reference filter of 620 nm. The analytical test was performed on 2 and 3 days after seeding cells on samples with diluted concentration. The cells cultured in medium without scaffolds served as control (100% cell viability).

2.5. Statistical analysis

Data were processed using Microsoft Excel 2016 software, and the results were presented as the mean \pm standard deviation of at least five experiments. The significance of the average values was calculated using a standard software program (SPSS GmbH, Munich, Germany) and $p \leq 0.05$ was considered significant.

3. Results and discussion

3.1. Morphological observation

A variety of factors, such as chemical composition, temperature, monomer concentration, solution pH, water-alcohol ratio, etc. are critical in the determination of final morphology and size distribution of the prepared spheres [38]. Fig. 1(a–e) indicate the FE-SEM micrographs and an average diameter of PDA nanospheres. The synthesized nanoparticles were fabricated by spontaneous oxidation of dopa-HCl under an alkaline condition at room temperature, with gentle stirring. The substantial factor in manufacturing PDA spheres is controlling the synthesizing process by addition of alcohol to the water-based solution. Thus, the effect of different alcohols (ethanol, isopropanol) was discussed in the present study. The obtained results demonstrated that

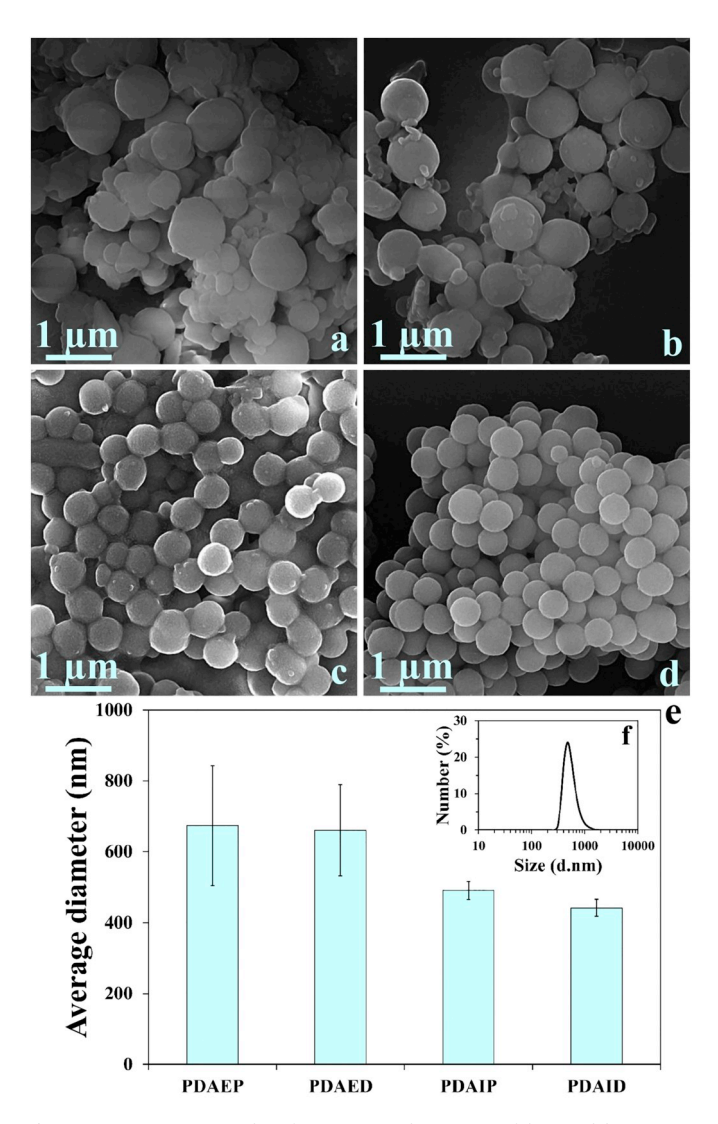


Fig. 1. FE-SEM micrographs of PDA nanospheres were fabricated by spontaneous oxidation in atmospheric air and alkaline condition (a–d) ((a) PDAEP, (b) PDAED, (c) PDAIP, (d) PDAID). The average diameter of PDA nanospheres in ethanol/isopropanol-water solution (e). The hydrodynamic diameter of PDAID nanospheres (f). Statistically significant differences were observed between groups except for PDAEP and PDAED.

uniform, monodisperse, and nanoscale PDA sphere-like shape were produced by isopropanol-water solution, while the degree of deformation in samples was represented in an ethanol-water solution that yielded larger diameter and size distribution in prepared mussel-inspired spheres, as listed in Table 1. Water to alcohol ratio will have a significant impression on monodispersity of the spheres, as Yan et al. [39] found out that the diameter of PDA spheres increased as a function of water content. Herein, the ratios 5:2 and 5:1 were selected for isopropanol and ethanol contained solutions, respectively, according to Hansen solubility parameters (HSP) theory. This theory thoroughly explains the logical reasons for selecting these ratios and the betterment of PDA morphology in isopropanol-contained solvents based on both Eqs. (1) and (2) [25]:

$$R_a = [4(D_{solv} - D_{solu})^2 + (P_{solv} - P_{solu})^2 + (H_{solv} - H_{solu})^2]^{0.5}$$
 (1)

$$D(PH)_{blend} = \sum \phi_{n.comp} D(PH)_{n.comp}$$
 (2)

where D, P, and H are dispersive, polar, and hydrogen bonding solubility parameter, respectively. R_a and Φ are the levels of conformity and the volume fraction of each composition, respectively. R_a value was

Table 3
Calculated-values based on HSP formula.

Code	The volume fraction of water	The volume fraction of alcohol	R_a
PDAED	83	17	3.23
PDAID	71	29	2.78

calculated in order to determine the water to alcohol ratio to achieve a possibly high solubility of the solvents. Table 3 represents calculated values based on HSP formula. Computed-data proved that the lower value of $R_{\rm a}$ in isopropanol-water mixed-solvent produced small, well-dispersed and monodisperse spheres.

Monomer addition is another challenge in the production of nanospheres. According to Fig. 1(a-d), uniform nanospheres with a smooth surface and tunable diameter were fabricated as a result of the dropwise addition of dopa-HCl to mixed solvent compared with a direct increment of monomer to the same solvent. Furthermore, size reduction of nanospheres should be considered when dopa-HCl is added to solvent dropwise. Obtained results led to selecting PDAID as a best-prepared sample for further investigations. The hydrodynamic diameter of PDAID nanospheres was measured by DLS analysis (Fig. 1f). According to the results, the average size was 476.7 nm with a low polydispersity index (0.151). It is clear that hydrodynamic size is larger than measured size in FE-SEM. Herein, adhesion of a thin electric dipole layer of solvent to nanospheres leading to measuring both core and solvent layer by DLS and indication of large size distribution. The same results were observed in other investigations [40,41]. Narrow size distribution confirmed the high degree of monodispersity of synthesized PDA nanospheres.

3.2. Polymerization

The FTIR spectra of the dopa-HCl and PDA are shown in Fig. 2a. Comparing the wavenumbers indicated the successful polymerization of dopamine. However, the change in color of the solution to brown can be the initial evidence of catechol oxidation during polymerization of dopa-HCl [14]. According to the FTIR spectrum, the broad peaks around 3000-3400 cm⁻¹ can be related to the intermolecular hydrogen bonds of dopa-HCl. The peaks at 2958, 3033, 3064, and 3145 cm⁻¹ are consistent with aromatic O-H asymmetry stretching vibration. Polymerization of dopa-HCl leads to changing NH2 in dopa-HCl into secondary amine [42] which the NH2 peaks are observed at 2432, 2538, 2638, 2746, and 3211 cm⁻¹ and disappeared after polymerization. Polymerization of monomer through spontaneous oxidation led to the formation of PDA nanospheres with intra/intermolecular cross-linking [15,39] via non-covalent interactions such as hydrogen bonding, $\pi-\pi$ stacking [8], hydrophobic interactions [43], and charge transfer [38]. For synthesized PDA, a broad peak at 3200-3500 cm⁻¹ is associated with the stretching vibration of phenolic O-H and N-H bonds related to catechol groups [13,44]. The absorption peak at 1603 cm⁻¹ indicates the aromatic ring and both stretching and bending vibration of N-H. The peaks at 1511 and 1119 cm⁻¹ are assigned to both N-H stretching vibration of the amide group and C-O vibration. The phenolic C-O-H bending and stretching vibration correlates with the peaks at 1344 and 1285 cm⁻¹, respectively [8]. Fig. 2b indicates the schematic of polymerization mechanism via spontaneous oxidation of dopamine hydrochloride. Briefly, the alkaline condition led to oxidation of dopa-HCl to dopaminequinone, then deprotonation of amine groups accompanied with 1,4-Michael addition resulting in the formation of leucodopaminechrome. After that, dopaminechrome was produced through oxidation of leucodopaminechrome. The rearrangement of the structure resulted in 5,6-dihydroxyindole, and finally, oquinone of 5,6-dihydroxyindole interacted with catechol groups to cross-link PDA [14,42]. It should be noticed that breakdown of 5,6dihydroxyindole is not extensive in nanosphere formation [45].

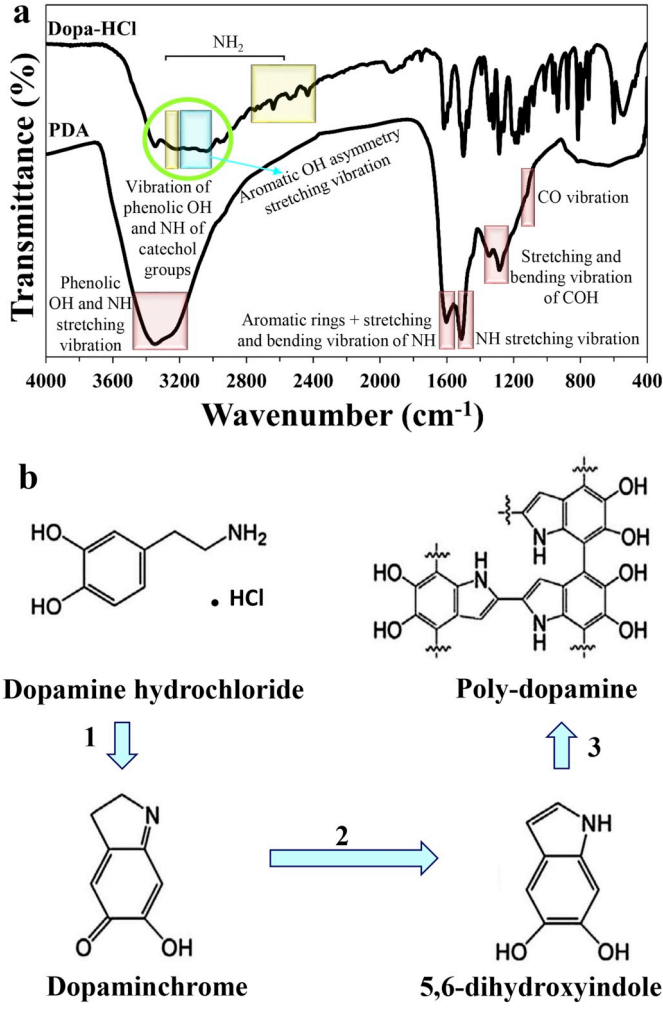


Fig. 2. Fourier transforms infrared spectroscopy of dopa.HCl and PDA (a), and a schematic of the polymerization level of dopa.HCl and cross-linking reaction (b). The steps of polymerization in the schematic are 1) oxidation, 2) rearrangement, and 3) polymerization.

As mentioned above, the pH is one of the serious parameters that affect polymerization of dopa-HCl. Conversion of dopa-HCl to PDA started via neutralization of acidic monomer by increasing pH till 8.5 with the addition of Tris-buffer [45]. Following the pH variation (Fig. 3a) during polymerization process indicated a gradual reduction of pH from 8.5 to 7.58 after three days of stirring owing to the abstraction of hydrogen atoms from dopa-HCl. This phenomenon may have occurred because of polymerization mechanism and ring closing reaction of monomer [46].

Fig. 3b illustrates the absorption peaks before and after polymerization through UV-vis spectrophotometer. UV-vis spectrum indicated peaks around 200–300 due to the conversion of dopa-HCl to 5,6-dihydroxyindole units [45]. An absorption peak around 280 nm in dopa-HCl is related to catechol groups in which its intensity decreased strongly after pH-induced polymerization [13,45]. Moreover, the peaks at 280 nm could be due to the lower tendency of small molecules to undergo oligomerization [47].

Fig. 3c demonstrates H-NMR spectroscopy of PDA. The observed peaks in NMR spectrum confirmed the polymerization dopa-HCl. The peaks around 1.4, 2.9 and 4 ppm are assigned to aliphatic protons such as (CH_2-C) , (CH_2-C/CH_2-N) and (CH_2-N) , respectively. Furthermore, aromatic CH related to indole were observed at 7 and 8.1 ppm, similar to the results of Liebscher et al. [48].

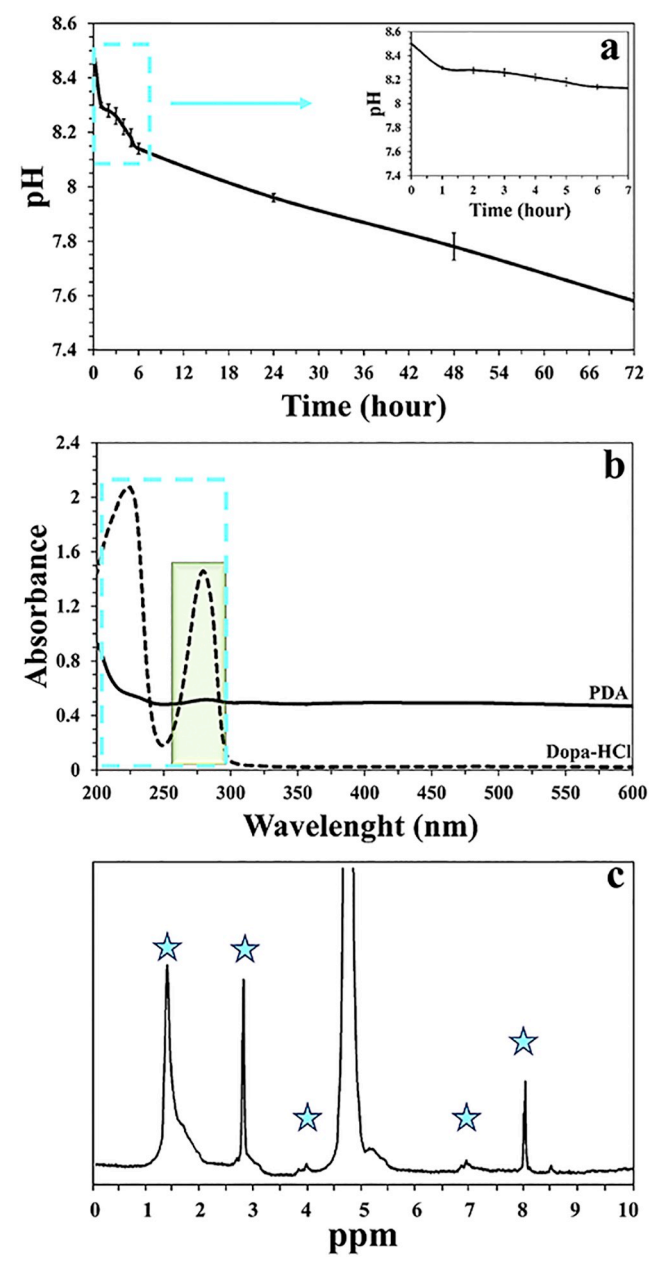


Fig. 3. Following the polymerization process. A variety of pH during a 3-day synthesizing process of PDA nanospheres (a), ultraviolet-visible absorption spectroscopy of dopa.HCl and PDA in the range of 200–600 nm (b), and proton nuclear magnetic resonance of PDA nanospheres (c).

3.3. Zeta potential

The zeta potential of prepared PDA nanospheres was measured at different pH (3, 5.5, 7, 8.5, and 10). Fig. 4a displays the change of surface charge in acidic, neutral, and alkaline solution. The surface charge in neutral solution was $-39.6 \pm 1.12 \,\mathrm{mv}$. By reducing pH to 5.5 and 3, charge repulsion increased to -26.8 ± 1.01 and $5.9 \pm 1.8 \,\mathrm{mv}$, respectively, and a positively charged sphere appeared in pH below 3 because of the protonation of the amino groups and the disappeared aromatic rings on PDA [8]. In contrast, higher pH values such as 8.5 and 10 induced negative surface charge ($-49.5 \pm 1.3 \,\mathrm{and} -55.7 \pm 1.5 \,\mathrm{mv}$, respectively) owing to the deprotonation of the phenolic groups of PDA nanospheres [8]. Moreover, the role of the dielectric constant of solvent in charge density of samples should not be ignored. For instance, Yu et al. [49], observed a reduction of charge

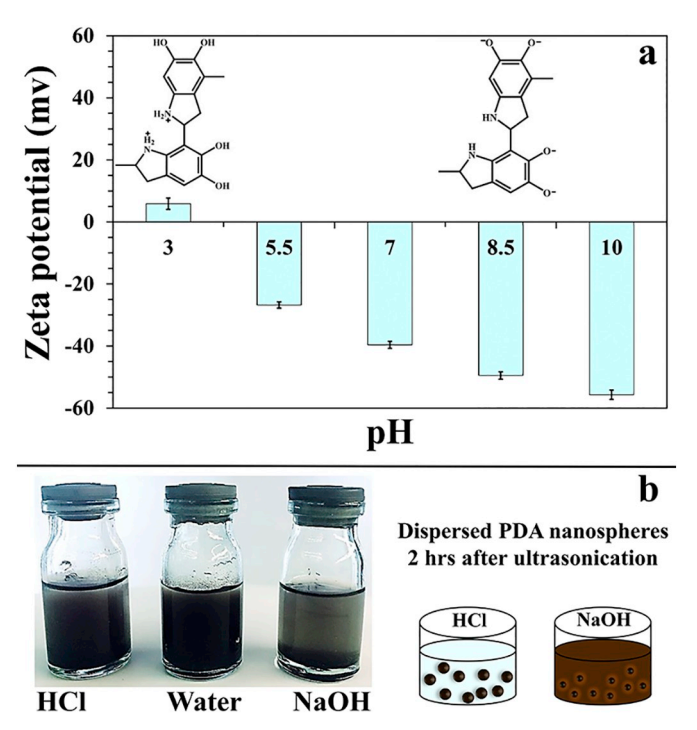


Fig. 4. Zeta potential of PDA nanospheres in different pH (3, 5.5, 7, 8.5, and 10) (a), and stability of PDA nanospheres in NaOH, DI-water and HCl 2h after ultrasonication (b).

density in ethanol compared with DI-water) the same pH) owing to a low dielectric constant of ethanol.

Fig. 4b shows the stability of PDA nanospheres in distinct solvents (NaOH, DI-water, and HCl) 2h after ultrasonication. Other investigation represented the excellent dispersion of PDA spheres in DI-water, ethanol, and *N*, *N*-dimethylformamide [39]. According to Fig. 4b, PDA nanosphere dispersed well in water and kept their stability after 2h because of intrinsic polar functional groups in the chemical structure of PDA such as -OH and C-O [13,15]. As Liu et al. [50] indicated that PDA capsules are stable within the pH range of 2–8.5. According to

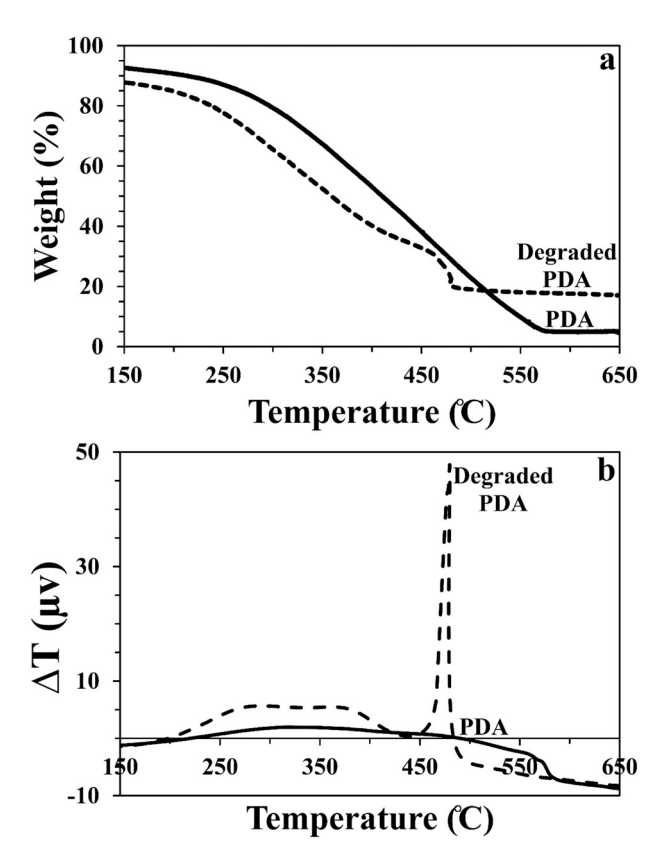


Fig. 6. TGA (a) and STA (b) analysis in an air atmosphere, temperature range from 150 to 650 $^{\circ}$ C, and a heating rate of 10 $^{\circ}$ C/min for the pure and degraded spheres.

Fig. 4b, the samples were stable under acidic condition more than several alkali conditions due to decomposition of spheres in higher pH provided by alkalis such as NaOH, KOH, etc. [39]. The difference in the behavior of PDA could be attributed to the different surface charge at various pH.

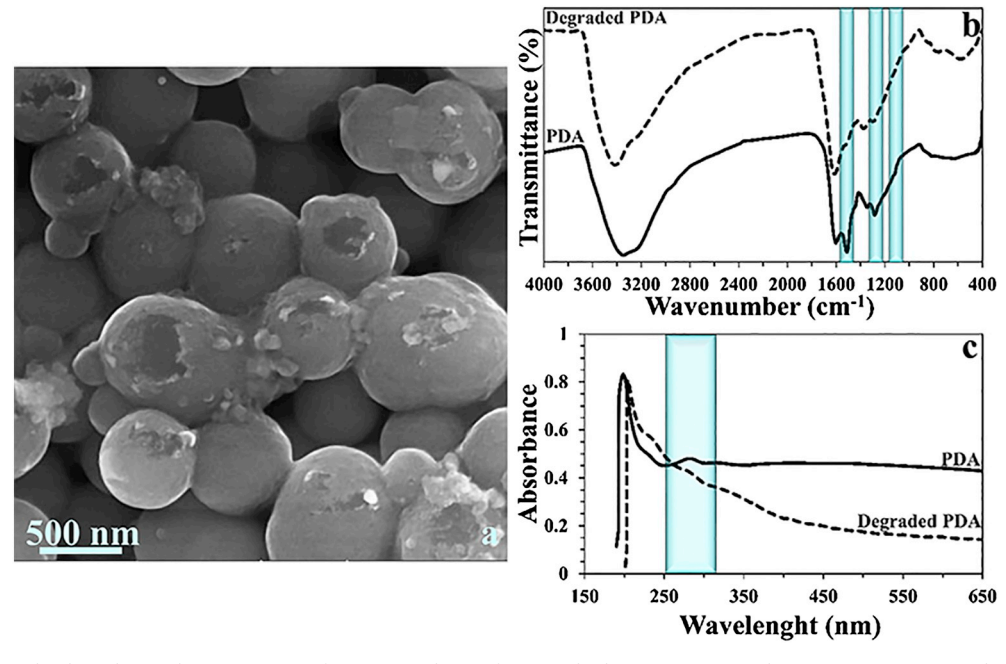


Fig. 5. In-vitro hydrolytic biodegradation characterization of PDA nanospheres after 4 weeks dispersion in PBS solution. FE-SEM micrographs (a), FTIR spectrum (b), UV-vis absorption spectrum in the range of 150–650 nm (c).

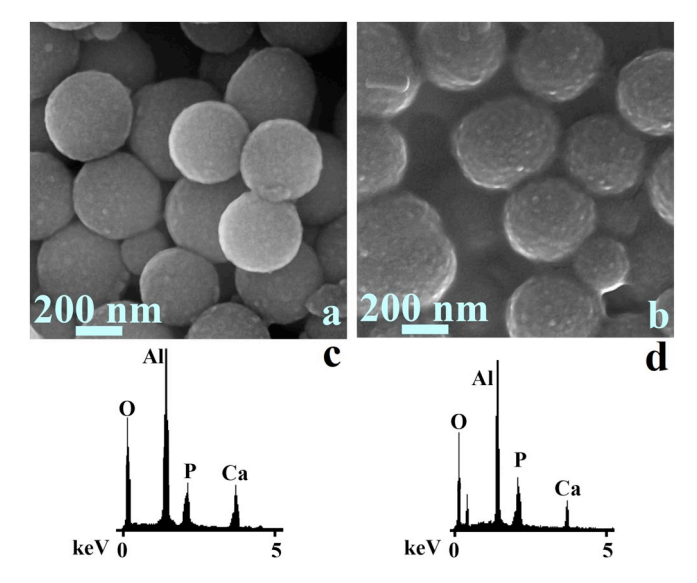


Fig. 7. In-vitro bioactive behavior of PDA nanospheres after 2 and 4 weeks dispersing in the SBF solution. FE-SEM micrographs and elemental analysis of the synthesized hydroxyapatite-like layers after 2 (a, c) and 4 (b, d) weeks.

3.4. In-vitro biodegradation

Biodegradation of biomedical materials and biocompatibility of their by-products is one of the critical issues in biomaterials studies. Chemical composition, hydrophilicity, surface area, size, shape, etc., of the constructs, are the determinants of biodegradation mechanism and its speed [51]. Researchers reported the presence of microorganisms, free radicals, and oxygen species provided by nicotinamide adenine dinucleotide phosphate oxidases through phagocytosis in the body which leads to oxidation of PDA and full in-vivo biodegradation during 8 weeks [52]. Figs. 5(a-c) and 6(a,b) illustrate the FE-SEM micrographs, FTIR spectrum, UV-vis absorption spectrum, TGA, and STA analysis of the degraded nanospheres after 4 weeks incubation in a PBS solution. As can be seen in the FE-SEM micrographs (Fig. 5a), the surface of the nanospheres were destroyed as a result of biodegradation. Reducing intensity and disappearance of absorption peaks at 1511 [53] and 1119 cm⁻¹ corroborated the degradation of N-H bonds in amide functional groups and aromatic carbons such as C=C and C=O bonds. Moreover, reducing peak intensity at 1285 cm⁻¹ can be assigned to C-O-H degradation that was observed by FTIR spectrum (Fig. 5b). Moreover, the destruction of the peak at 280 nm in UV-vis spectrum (Fig. 5c) is related to the degradation of catechol groups. TGA analysis (Fig. 6a) was performed in the range of 150-650 °C and showed thermal stability of PDA in high temperature. As represented in Fig. 6a the PDA

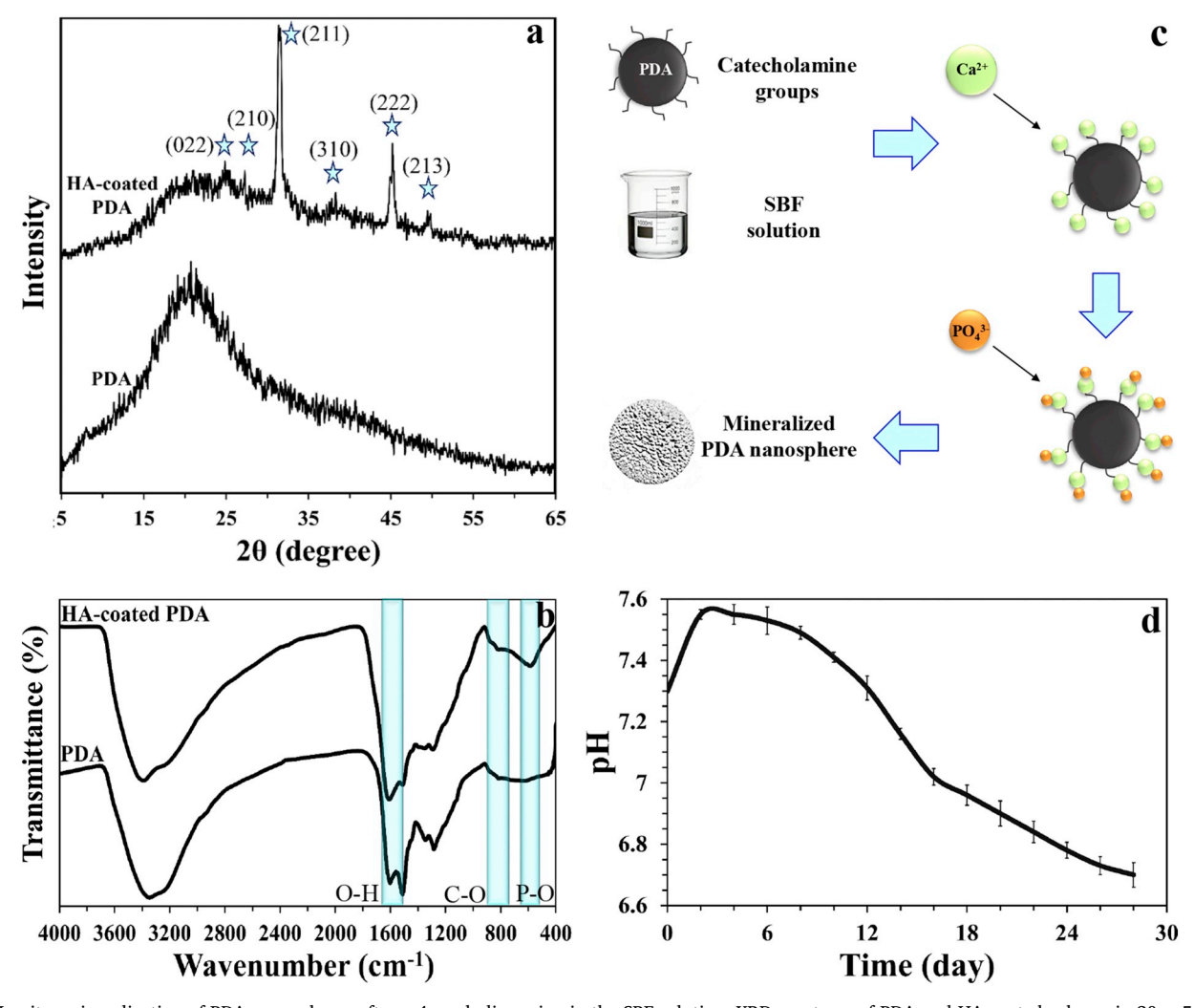


Fig. 8. In-vitro mineralization of PDA nanospheres after a 4-week dispersing in the SBF solution. XRD spectrum of PDA and HA-coated spheres in $2\theta = 5-65^{\circ}$ (a), FTIR spectrum (c) of pure and mineralized PDA, schematic of mineralization of PDA nanospheres in SBF solution (c), and the variety of pH during a 28-day biomineralization (d).

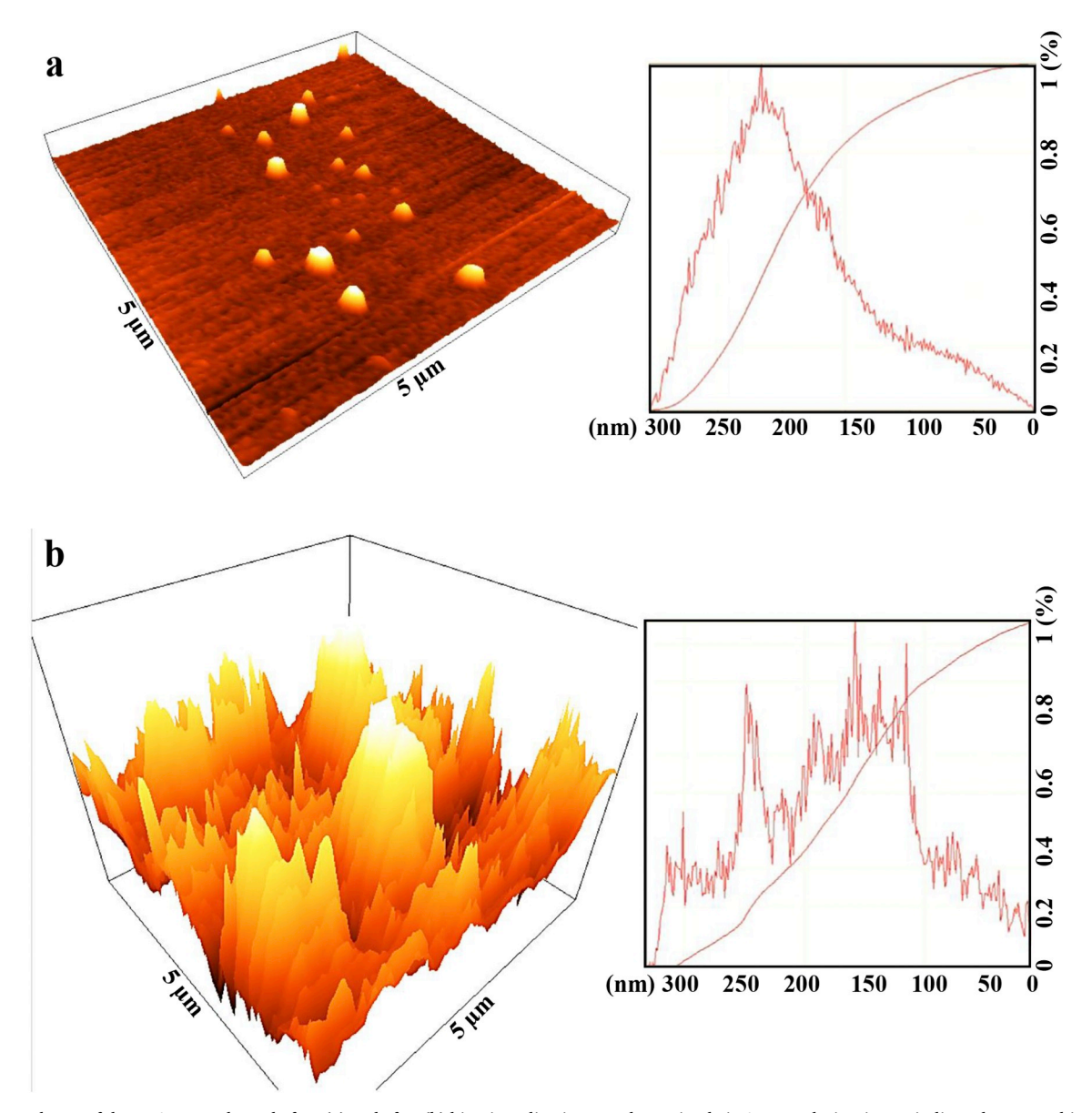


Fig. 9. The roughness of the PDA nanospheres before (a) and after (b) biomineralization was determined via AFM analysis. Figures indicated topographic observation and high distribution diagram of nanospheres.

nanospheres degraded at about 574 $^{\circ}$ C and this temperature reduced to 481 $^{\circ}$ C for a 4-week degraded spheres. The stable line slope after this temperature indicated destroying the structure of test samples. PDA nanospheres which passed biodegradation analysis lost their weight in TGA analysis faster than pure PDA nanospheres owing to the destruction of the chemical groups after degradation time. The stability of the slope of the diagram (biodegraded PDA) after about 480 $^{\circ}$ C confirmed this occurrence.

Moreover, observing a broad peak around $150-400\,^{\circ}\mathrm{C}$ in STA spectrum (Fig. 6b) of nanoparticles before and after degradation can be attributed to the water loss associated with hydrophilic groups and thermal decomposition of amine groups while its intensity reduced after biodegradation in PBS solution due to degradation of the mentioned functional groups. The sharp peak at $480\,^{\circ}\mathrm{C}$ in degraded samples confirmed the complementation of TGA analysis and complete degradation of samples because of heat up in these analyses.

3.5. In-vitro bioactivity

Biomimetic formation of HA was accompanied by immersion of PDA

nanospheres into SBF solution for 2 and 4 weeks. Synthesized HA on the surface of bio-inspired PDA were characterized via several analytical assays such as FE-SEM micrographs, XRD spectrum, EDX analysis, pH measurement, FTIR spectrum and AFM test as shown in Figs. 7(a–d), 8(a–d), and 9(a,b). FE-SEM images (Fig. 7(a,b)) confirmed the formation of hybrid organic-inorganic nanospheres through layer by layer and monotonic biomineralization of calcium phosphates on the surface of bioactive template particles [32]. According to the figures, the density of mineralized layer on the surface increased from day 14 to 28.

The elemental characterization of biomimetic HA was indicated by EDX test (Fig. 7c). Observation of Ca and P peaks after soaking PDA in SBF solution was evidence of complete coverage of samples with HA. Furthermore, Ca/P weight ratio of the mineralized layer was approximately 1.79 and 1.95 after a 14 and 28-day immersion in SBF solution. Based on the obtained results, the mineralization increased as a function of increasing soaking time. However, The lower ratio of Ca/P compared with biological HA could be because of structural differences and lack of adequate carbonate, sodium and magnesium ions in the composition of prepared HA. Similar results were observed by Cui et al. [33].

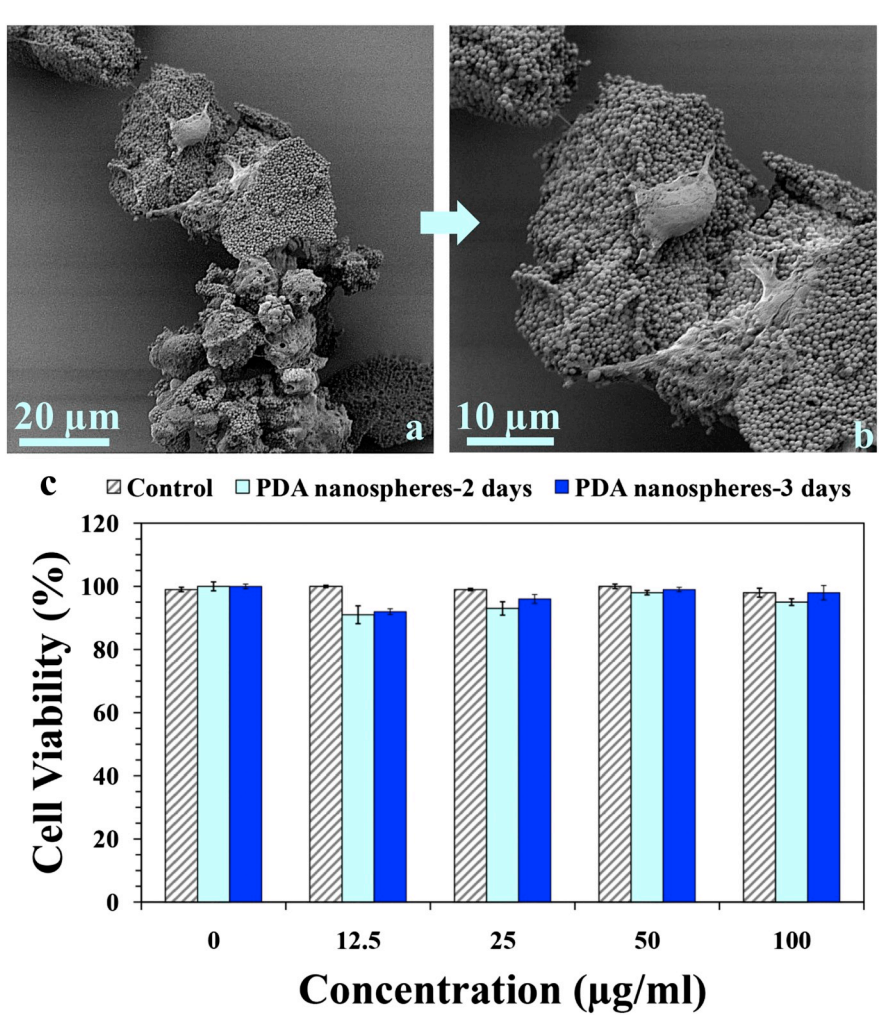


Fig. 10. FE-SEM micrographs of L929 mouse fibroblast cells attachment on PDA nanospheres (a, b), and viability of L929 fibroblast cells in the presence of ascending concentration (0, 12.5, 25, 50, and 100 μg/mL) of PDA during a 2-day and 3-day culturing (c). There are no statistically significant differences between groups.

Moreover, XRD spectrum (Fig. 8a) proved that these mineralized layers were hydroxyapatite. Amorphous structure of PDA led to observation of a broad peak at 20 angles around 10–30°. Soaking the samples in Kokubo SBF strongly decreased the intensity of amorphous peak and exposed the major HA characteristic peaks at 20 angles of 25.27, 27.27, 31.55, 39.65, 45.62, and 49.53° corresponding to reflection of (002), (210), (211), (310), (222), and (213) crystals [54,55]. It should be noted that amorphous nature of PDA and nanocrystalline growth of HA propelled to displaying broad peaks in spectrum.

FTIR spectrum of SBF-immersed spheres is shown in Fig. 8b. The appearance of a peak at the 582 cm⁻¹ is related to the bending vibration of P-O bonds in tetrahedral phosphate [56]. Slight peaks at 819 cm⁻¹ demonstrate C-O vibration of synthesized HA [57]. Increasing the intensity of the peak at 1603 cm⁻¹ is attributed to O-H stretching [58].

Fig. 8c indicated the schematic of apatite formation. pH measurement (Fig. 8d) during mineralization of mussel-inspired particles presented a slight increase in the pH till 3 days after soaking the constructs in SBF solution. This phenomenon could be due to release of H⁺ from hydroxyl groups of PDA into SBF solution and sedimentation of acidic components such as HCO³⁻ and HPO₄²⁻ [59] on the surface of the spheres as a stimulator of CaP nucleation. Ca²⁺ ions were transferred to PDA surface, and hemispherical CaP agglomerates were created [32], so it led to a reduction in pH till the end of the experiment. Based on Fig. 4a, PDA nanospheres have a negative surface charge at physiologic pH. So, they show a great tendency to attract metal ions in SBF solution

and decrease the energy of the system. Charge repulsion and presence of abundant free catecholamine moieties [32,38] after polymerization (Fig. 3b) result in the precipitation of ${\rm Ca}^{2^+}$ ions at the interface of bioactive spheres and SBF solution. Absorption of calcium ions in nucleation sites leads to deposition of ${\rm HPO_4}^{2^-}$ and rapid growth of CaP layers [59].

Surface roughness before and after mineralization was studied by AFM analysis. Fig. 9(a,b) indicated approximately uniform and homogeneous topography for all the spheres while the thickness increased as a function of incubation in SBF solution. Maximum height in the direction of z-axis was reached from 304 to 331 nm and proved the changing topography as a result of apatite formation. Additionally, S_q parameter increased from 61 to 74.7 nm.

3.6. Cells-spheres interactions

Cell culture experiments provide valuable information about cell-sample interactions, physiology and chemistry of cells, toxicity, mutagenesis, and carcinogenesis ability of materials or by-products. Moreover, they are widely used for testing biological components and simulating in-vivo reactions. Therefore, biocompatibility of the PDA nanospheres was investigated through culturing of L929 mouse fibroblast cells (Fig. 10(a–c)). The results of FE-SEM test (Fig. 10(a,b)) illustrated that polymeric nanoparticles could support cellular adhesion and spread. PDA samples can act as a bioadhesive in water [22] and prevent protein denaturation for the betterment of cell adhesion [38].

In fact, the presence of amine and a hydroxyl group in the chemical structure of PDA play an unbelievable role in the absorption of fibronectin in serum, leading to the introduction of cell anchorage sites. Besides, the hydrophilicity of PDA allows more interactions with integrin to improve adhesion and growth [23].

Cytotoxicity of cell-loaded samples was studied by MTT assay on ascending concentrations of PDA. Dehydrogenase activity of mitochondrial and cellular respiration cycle indicated a number of viable cells via MTT assay. According to Fig. 10c, the constructs showed desirable biocompatibility and cellular growth owing to lack of stresses and presence of nutrients-rich media [60,61]. According to the results, the number of living cells was slightly reduced by increasing the concentration of nanoparticles to $100\,\mu\text{g/mL}$, but the viability of >90% cells in both time points compared to control group confirmed the synthesizing biocompatible bio-inspired structure for biomedical applications, such as other investigations [62,63]. Additionally, results demonstrated an increasing number of living cells as a function of increasing incubation time and confirmed the ability of PDA nanospheres for supporting the proliferation of cells. A large number of viable cells in cell culture plate was used as control group.

4. Conclusion

In brief, bioactive inspired PDA nanospheres were synthesized via spontaneous oxidative polymerization of dopamine hydrochloride (dopa-HCl) under an alkaline condition at ambient temperature, atmospheric air, and an alkaline condition. Production of uniform and monodisperse spheres with tunable nanoscale size was made possible by the dropwise addition of a monomer in isopropanol-water mixed solution. Bioactive sites in mussel-inspired spheres support the formation of HA and fabrication of hybrid organic-inorganic nanospheres. The ability of PDA in the attraction of adhesive proteins in serum created an acceptable surface for cellular adhesion. Finally, it is believed that biocompatible PDA nanospheres are promising potential candidates for biomedical applications.

References

- B. Ratner, A. Hoffman, F. Schoen, J. Lemons, Biomaterials Science: An Introduction to Materials in Medicine, 2nd ed., (2013).
- [2] G. Wei, J. Zhang, L. Xie, K.D. Jandt, Biomimetic growth of hydroxyapatite on super water-soluble carbon nanotube-protein hybrid nanofibers, Carbon N. Y. 49 (2011) 2216–2226, https://doi.org/10.1016/j.carbon.2011.01.051.
- [3] A.G.B. Castro, M. Diba, M. Kersten, J.A. Jansen, J.J.J.P. van den Beucken, F. Yang, Development of a PCL-silica nanoparticles composite membrane for Guided Bone Regeneration, Mater. Sci. Eng. C 85 (2018) 154–161, https://doi.org/10.1016/j. msec.2017.12.023.
- [4] P. Gong, S. Ji, J. Wang, D. Dai, F. Wang, M. Tian, L. Zhang, F. Guo, Z. Liu, Fluorescence-switchable ultrasmall fluorinated graphene oxide with high near-infrared absorption for controlled and targeted drug delivery, Chem. Eng. J. 348 (2018) 438–446, https://doi.org/10.1016/j.cej.2018.04.193.
- [5] L. Wang, Y. Wu, J. Xie, S. Wu, Z. Wu, Characterization, antioxidant and antimicrobial activities of green synthesized silver nanoparticles from *Psidium guajava* L. leaf aqueous extracts, Mater. Sci. Eng. C 86 (2018) 1–8, https://doi.org/10.1016/ j.msec.2018.01.003.
- [6] Z. Song, Y. Liu, J. Shi, T. Ma, Z. Zhang, H. Ma, S. Cao, Hydroxyapatite/mesoporous silica coated gold nanorods with improved degradability as a multi-responsive drug delivery platform, Mater. Sci. Eng. C 83 (2018) 90–98, https://doi.org/10.1016/j. msec.2017.11.012.
- [7] C. Qiao, J. Yang, L. Chen, J. Weng, X. Zhang, Intracellular accumulation and immunological responses of lipid modified magnetic iron nanoparticles in mouse antigen processing cells, Biomater. Sci. 5 (2017) 1603–1611, https://doi.org/10.1039/C7BM00244K.
- [8] J. Fu, Z. Chen, M. Wang, S. Liu, J. Zhang, J. Zhang, R. Han, Q. Xu, Adsorption of methylene blue by a high-efficiency adsorbent (polydopamine microspheres): kinetics, isotherm, thermodynamics and mechanism analysis, Chem. Eng. J. 259 (2015) 53–61, https://doi.org/10.1016/j.cej.2014.07.101.
- [9] F. Group, Nanobiomaterials Handbook, CRC Press, 2011, https://doi.org/10.1201/ b10970.
- [10] A.R. Boccaccini, P.X. Ma, Tissue Engineering Using Ceramics and Polymers, (2014).
- [11] S.M. Davachi, B. Kaffashi, B. Torabinejad, A. Zamanian, J. Seyfi, I. Hejazi, Investigating thermal, mechanical and rheological properties of novel antibacterial hybrid nanocomposites based on PLLA/triclosan/nano-hydroxyapatite, Polymer (Guildf.) 90 (2016) 232–241, https://doi.org/10.1016/j.polymer.2016.03.007.

- [12] M.M. Safikhani, A. Zamanian, F. Ghorbani, A. Asefnejad, M. Shahrezaee, Bi-layered electrospun nanofibrous polyurethane-gelatin scaffold with targeted heparin release profiles for tissue engineering applications, J. Polym. Eng. 37 (2017), https://doi. org/10.1515/polyeng-2016-0291.
- [13] H. Luo, C. Gu, W. Zheng, F. Dai, X. Wang, Z. Zheng, Facile synthesis of novel size-controlled antibacterial hybrid spheres using silver nanoparticles loaded with poly-dopamine spheres, RSC Adv. 5 (2015) 13470–13477, https://doi.org/10.1039/C4RA16469E.
- [14] Q. Wei, F.L. Zhang, J. Li, B.J. Li, C.S. Zhao, Oxidant-induced dopamine polymerization for multifunctional coatings, Polym. Chem. 1 (2010) 1430–1433, https://doi.org/10.1039/c0py00215a.
- [15] S. Xiong, Y. Wang, J. Yu, L. Chen, J. Zhu, Z. Hu, Polydopamine particles for next-generation multifunctional biocomposites, J. Mater. Chem. A 2 (2014) 7578–7588, https://doi.org/10.1039/c4ta00235k.
- [16] M. Lai, Z. Jin, Z. Su, Surface modification of TiO2 nanotubes with osteogenic growth peptide to enhance osteoblast differentiation, Mater. Sci. Eng. C 73 (2017) 490–497, https://doi.org/10.1016/j.msec.2016.12.083.
- [17] C. Xie, P. Li, L. Han, Z. Wang, T. Zhou, W. Deng, K. Wang, X. Lu, Electroresponsive and cell-affinitive polydopamine/polypyrrole composite microcapsules with a dualfunction of on-demand drug delivery and cell stimulation for electrical therapy, NPG Asia Mater. 9 (2017) e358, https://doi.org/10.1038/am.2017.16.
- [18] J. Zhou, X. Guo, Q. Zheng, Y. Wu, F. Cui, B. Wu, Improving osteogenesis of three-dimensional porous scaffold based on mineralized recombinant human-like collagen via mussel-inspired polydopamine and effective immobilization of BMP-2-derived peptide, Colloids Surf. B: Biointerfaces 152 (2017) 124–132, https://doi.org/10.1016/j.colsurfb.2016.12.041.
- [19] C. Jiang, Y. Wang, J. Wang, W. Song, L. Lu, Achieving ultrasensitive in vivo detection of bone crack with polydopamine-capsulated surface-enhanced Raman nanoparticle, Biomaterials 114 (2017) 54–61, https://doi.org/10.1016/j.biomaterials. 2016.11.007.
- [20] Y. Hu, W. Dan, S. Xiong, Y. Kang, A. Dhinakar, J. Wu, Z. Gu, Development of collagen/polydopamine complexed matrix as mechanically enhanced and highly biocompatible semi-natural tissue engineering scaffold, Acta Biomater. 47 (2017) 135–148, https://doi.org/10.1016/j.actbio.2016.10.017.
- [21] X. Zhao, Y. Han, J. Li, B. Cai, H. Gao, W. Feng, S. Li, J. Liu, D. Li, BMP-2 immobilized PLGA/hydroxyapatite fibrous scaffold via polydopamine stimulates osteoblast growth, Mater. Sci. Eng. C (2017), https://doi.org/10.1016/j.msec.2017.03.186.
- [22] A. Liu, L. Zhao, H. Bai, H. Zhao, X. Xing, G. Shi, Polypyrrole actuator with a bioadhesive surface for accumulating bacteria from physiological media, ACS Appl. Mater. Interfaces 1 (2009) 951–955, https://doi.org/10.1021/am9000387.
- [23] M. Liu, J. Zhou, Y. Yang, M. Zheng, J. Yang, J. Tan, Surface modification of zirconia with polydopamine to enhance fibroblast response and decrease bacterial activity in vitro: a potential technique for soft tissue engineering applications, Colloids Surf. B: Biointerfaces 136 (2015) 74–83, https://doi.org/10.1016/j.colsurfb.2015.06.047.
- [24] F. Gong, J. Zhang, L. Ding, Z. Yang, X. Liu, Mussel-inspired coating of energetic crystals: a compact core-shell structure with highly enhanced thermal stability, Chem. Eng. J. 309 (2017) 140–150, https://doi.org/10.1016/j.cej.2016.10.020.
- 25] X. Jiang, Y. Wang, M. Li, Selecting water-alcohol mixed solvent for synthesis of polydopamine nano-spheres using solubility parameter, Sci. Rep. 4 (2014) 6070, https://doi.org/10.1038/srep06070.
- [26] S. Hesaraki, A. Zamanian, F. Moztarzadeh, Effect of adding sodium hexametaphosphate liquefier on basic properties of calcium phosphate cements, J. Biomed. Mater. Res. A 88A (2009) 314–321, https://doi.org/10.1002/jbm.a.31836.
- [27] G. Wei, J. Reichert, J. Bossert, K.D. Jandt, Novel biopolymeric template for the nucleation and growth of hydroxyapatite crystals based on self-assembled fibrinogen fibrils, Biomacromolecules 9 (2008) 3258–3267, https://doi.org/10. 1021/bm800824r
- [28] J. Wang, Z. Ouyang, Z. Ren, J. Li, P. Zhang, G. Wei, Z. Su, Self-assembled peptide nanofibers on graphene oxide as a novel nanohybrid for biomimetic mineralization of hydroxyapatite, Carbon N. Y. 89 (2015) 20–30, https://doi.org/10.1016/j. carbon.2015.03.024.
- [29] H. Qu, M. Wei, The effect of temperature and initial pH on biomimetic apatite coating, J Biomed Mater Res B Appl Biomater 87B (2008) 204–212, https://doi. org/10.1002/jbm.b.31096.
- [30] N. Arabi, A. Zamanian, Effect of cooling rate and gelatin concentration on the microstructural and mechanical properties of ice template gelatin scaffolds, Biotechnol. Appl. Biochem. 60 (2013) 573–579, https://doi.org/10.1002/bab. 1120
- [31] A. Zamanian, S. Farhangdoust, M. Yasaei, M. Khorami, M. Hafezi, The effect of particle size on the mechanical and microstructural properties of freeze-casted macroporous hydroxyapatite scaffolds, Int. J. Appl. Ceram. Technol. 11 (2014) 12–21, https://doi.org/10.1111/ijac.12031.
- [32] J. Ryu, S.H. Ku, H. Lee, C.B. Park, Mussel-inspired polydopamine coating as a universal route to hydroxyapatite crystallization, Adv. Funct. Mater. 20 (2010) 2132–2139, https://doi.org/10.1002/adfm.200902347.
- [33] J. Cui, C. Ma, Z. Li, L. Wu, W. Wei, M. Chen, B. Peng, Z. Deng, Polydopamine-functionalized polymer particles as templates for mineralization of hydroxyapatite: biomimetic and in vitro bioactivity, RSC Adv. 6 (2016) 6747–6755, https://doi.org/10.1039/c5ra24821c.
- [34] W. Zhe, C. Dong, Y. Sefei, Z. Dawei, X. Kui, L. Xiaogang, Facile incorporation of hydroxyapatite onto an anodized Ti surface via a mussel inspired polydopamine coating, Appl. Surf. Sci. 378 (2016) 496–503, https://doi.org/10.1016/j.apsusc. 2016.2.004
- [35] Y.-L. Cheng, Y.-W. Chen, K. Wang, M.-Y. Shie, Enhanced adhesion and differentiation of human mesenchymal stem cell inside apatite-mineralized/poly

- (dopamine)-coated poly(e-caprolactone) scaffolds by stereolithography, J. Mater. Chem. B 4 (2016) 6307–6315, https://doi.org/10.1039/C6TB01377E.
- [36] T. Kokubo, H. Takadama, How useful is SBF in predicting in vivo bone bioactivity? Biomaterials 27 (2006) 2907–2915, https://doi.org/10.1016/j.biomaterials.2006. 01.017.
- [37] P. Gong, Q. Zhao, D. Dai, S. Zhang, Z. Tian, L. Sun, J. Ren, Z. Liu, Functionalized ultrasmall fluorinated graphene with high NIR absorbance for controlled delivery of mixed anticancer drugs, Chem. Eur. J. 23 (2017) 17531–17541, https://doi.org/10. 1002/chem.201702917.
- [38] Y.H. Ding, M. Floren, W. Tan, Mussel-inspired polydopamine for bio-surface functionalization, Biosurf. Biotribol. 2 (2016) 121–136, https://doi.org/10.1016/j.bsbt. 2016.11.001.
- [39] J. Yan, L. Yang, M.-F. Lin, J. Ma, X. Lu, P.S. Lee, Polydopamine spheres as active templates for convenient synthesis of various nanostructures, Small 9 (2013) 596–603, https://doi.org/10.1002/smll.201201064.
- [40] W. Zheng, F. Gao, H. Gu, Magnetic polymer nanospheres with high and uniform magnetite content, J. Magn. Magn. Mater. 288 (2005) 403–410, https://doi.org/10. 1016/j.jmmm.2004.09.125.
- [41] Y. Chen, E.T. Kang, K.G. Neoh, A. Greiner, Preparation of hollow silica nanospheres by surface-initiated atom transfer radical polymerization on polymer latex templates, Adv. Funct. Mater. 15 (2005) 113–117, https://doi.org/10.1002/adfm. 200400179
- [42] F. Yu, S. Chen, Y. Chen, H. Li, L. Yang, Y. Chen, Y. Yin, Experimental and theoretical analysis of polymerization reaction process on the polydopamine membranes and its corrosion protection properties for 304 stainless steel, J. Mol. Struct. 982 (2010) 152–161, https://doi.org/10.1016/j.molstruc.2010.08.021.
- [43] Z. Iqbal, E.P.C. Lai, T.J. Avis, Antimicrobial effect of polydopamine coating on Escherichia coli, J. Mater. Chem. 22 (2012) 21608–21613, https://doi.org/10.1039/ c2im34825i.
- [44] N. Nishizawa, A. Kawamura, M. Kohri, Y. Nakamura, S. Fujii, Polydopamine particle as a particulate emulsifier, Polymers (Basel) 8 (2016) 62–77, https://doi.org/10.3390/polym8030062.
- [45] J.-H. Lin, C.-J. Yu, Y.-C. Yang, W.-L. Tseng, Formation of fluorescent polydopamine dots from hydroxyl radical-induced degradation of polydopamine nanoparticles, Phys. Chem. Chem. Phys. 17 (2015) 15124–15130, https://doi.org/10.1039/ c5cn00932d.
- [46] K. Ju, Y. Lee, S. Lee, S.B. Park, J. Lee, Bioinspired polymerization of dopamine to generate melanin-like nanoparticles having an excellent free-radical-scavenging property, Biomacromolecules 12 (2011) 625–632.
- [47] F. Bernsmann, A. Ponche, C. Ringwald, J. Hemmerlé, J. Raya, B. Bechinger, J. Voegel, P. Schaaf, V. Ball, Characterization of dopamine – melanin growth on silicon oxide, J. Phys. Chem. C 113 (2009) 8234–8242, https://doi.org/10.1021/ ip901188h
- [48] J. Liebscher, R. Mrówczyński, H.A. Scheidt, C. Filip, N.D. Haidade, R. Turcu, A. Bende, S. Beck, Structure of polydopamine: a never-ending story? Langmuir 29 (2013) 10539–10548. https://doi.org/10.1021/la4020288.
- [49] B. Yu, D.A. Wang, Q. Ye, F. Zhou, W. Liu, Robust polydopamine nano/micro-capsules and their loading and release behavior, Chem. Commun. (Camb.) (44) (2009) 6789–6791, https://doi.org/10.1039/b910679k.

- [50] Q. Liu, B. Yu, W. Ye, F. Zhou, Highly selective uptake and release of charged molecules by pH-responsive polydopamine microcapsules, Macromol. Biosci. 11 (2011) 1227–1234, https://doi.org/10.1002/mabi.201100061.
- [51] J.M. Anderson, M.S. Shive, Biodegradation and biocompatibility of PLA and PLGA microspheres, Adv. Drug Deliv. Rev. 64 (2012) 72–82, https://doi.org/10.1016/j. addr.2012.09.004.
- [52] Y. Liu, K. Ai, L. Lu, Polydopamine and its derivative materials: synthesis and promising applications in energy, environmental, and biomedical fields, Chem. Rev. 114 (2014) 5057–5115, https://doi.org/10.1021/cr400407a.
- [53] D. Hong, H. Lee, B.J. Kim, T. Park, J.Y. Choi, M. Park, J. Lee, H. Cho, S.-P. Hong, S.H. Yang, S.H. Jung, S.-B. Ko, I.S. Choi, A degradable polydopamine coating based on disulfide-exchange reaction, Nanoscale 7 (2015) 20149–20154, https://doi.org/ 10.1039/C5NR06460K.
- [54] D. Yaoke, Z. Yuan, J. Wang, Synthesis of a phosphorus-containing trisilanol POSS and its application in RTV composites, E-Polymers 18 (2018) 237–245, https://doi. org/10.1515/epoly-2017-0204.
- [55] F. Ghorbani, A. Zamanian, A. Behnamghader, M. Daliri Joupari, A novel pathway for in situ synthesis of modified gelatin microspheres by silane coupling agents as a bioactive platform, J. Appl. Polym. Sci. (2018) 46739, https://doi.org/10.1002/app.46739.
- [56] F.H. El-Batal, A.A. El-Kheshen, Y.M. Hamdy, Absorption spectra and bioactivity behavior of gamma irradiated CeO2-doped bioglasses, SILICON 5 (2013) 171–181, https://doi.org/10.1007/s12633-012-9112-4.
- [57] A. Li, H. Shen, H. Ren, C. Wang, D. Wu, R.A. Martin, D. Qiu, Bioactive organic/inorganic hybrids with improved mechanical performance, J. Mater. Chem. B 3 (2015) 1379–1390, https://doi.org/10.1039/C4TB01776E.
- [58] F. Ghorbani, A. Zamanian, A. Behnamghader, M.D. Joupari, Microwave-induced rapid formation of biomimetic hydroxyapatite coating on gelatin-siloxane hybrid microspheres in 10X-SBF solution, E-Polymers (2018), https://doi.org/10.1515/ epoly-2017-0196.
- [59] M. Áraújo, M. Miola, E. Bertone, G. Baldi, J. Perez, E. Verné, On the mechanism of apatite-induced precipitation on 45S5 glass pellets coated with a natural-derived polymer, Appl. Surf. Sci. 353 (2015) 137–149, https://doi.org/10.1016/j.apsusc. 2015.06.088.
- [60] F. Ghorbani, A. Zamanian, H. Nojehdehian, Effects of pore orientation on in-vitro properties of retinoic acid-loaded PLGA/gelatin scaffolds for artificial peripheral nerve application, Mater. Sci. Eng. C 77 (2017) 159–172, https://doi.org/10.1016/ j.msec.2017.03.175.
- [61] M.M. Safikhani, A. Zamanian, F. Ghorbani, Synergistic effects of retinoic acid and graphene oxide on the physicochemical and in-vitro properties of electrospun polyurethane scaffolds for bone tissue engineering, E-Polymers 17 (2017) 363–371, https://doi.org/10.1515/epoly-2016-0304.
- [62] P. Gong, L. Guo, M. Pang, D. Wang, L. Sun, Z. Tian, J. Li, Y. Zhang, Z. Liu, Nano-sized paramagnetic and fluorescent fluorinated carbon fiber with high NIR absorbance for cancer chemo-photothermal therapy, J. Mater. Chem. B 6 (2018) 3068–3077, https://doi.org/10.1039/c7tb03320f.
- [63] L. Sun, P. Gong, X. Liu, M. Pang, M. Tian, J. Chen, J. Du, Z. Liu, Fluorinated carbon fiber as a novel nanocarrier for cancer chemo-photothermal therapy, J. Mater. Chem. B 5 (2017) 6128–6137, https://doi.org/10.1039/c7tb01155e.